Submitted: 26 June, 2023 Accepted: 23 August, 2023 Published: 15 February, 2025 DOI:10.22514/ejgo.2023.072

ORIGINAL RESEARCH

European Journal of Gynaecological Oncology

Identification of an immune-related metabolic gene signature to predict possible prognosis in endometrial cancer and reveals immune landscape feature

Yuemei Cheng[1], Pingyuan Yu[1], Xiaolei Liang[2], Yongxiu Yang[2,*]

[1]The First Clinical Medical College of Lanzhou University, Key Laboratory of Gynecological Oncology of Gansu Province, 730000 Lanzhou, Gansu, China
[2]Department of Obstetrics and Gynecology, The First Hospital of Lanzhou University, Key Laboratory of Gynecologic Oncology of Gansu Province, 730000 Lanzhou, Gansu, China

***Correspondence**
yangyx@lzu.edu.cn
(Yongxiu Yang)

Abstract

Background: The immunotherapy of endometrial cancer (EC) has gradually attracted attention and metabolic reprogramming is associate with tumor immune infiltration. Our goal was to use proteome analysis to examine the role of immune-related metabolic genes (IRMGs) in EC. **Methods**: Data-independent acquisition mass spectrometry (DIA-MS) was performed on 20 EC patients, consisting of 10 high-grade and 10 low-grade cancer tissues. IRMGs were screened using Spearman correlation, and an immune-related metabolic prognosis signature (IRMPS) was constructed based on the Cancer Genome Atlas-Uterine Corpus Endometrioid Carcinoma (TCGA-UCEC) cohort using the least absolute shrinkage and selection operator (LASSO) regression analysis. We also investigated differences between different risk groups in terms of prognostic value, clinical potency, immune characteristics and therapy response. **Results**: In total, 285 differentially expressed genes (DEGs) were acquired via DIA-MS. Subsequently, metabolic-DEGs and immune-DEGs were analyzed by Spearman correlation to identify 41 IRMGs. Finally, seven IRMGs, including NADH dehydrogenase (ubiquinone) 1 alpha subcomplex subunit 2 (*NDUFA2*), AMPK-alpha2 (*PRKAA2*), syntaxin binding protein 1 (*STXBP1*), NADH dehydrogenase (ubiquinone) 1 beta subcomplex subunit 9 (*NDUFB9*), ribosomal protein S27-like (*RPS27L*), lysolecithin acyltransferase 2 (*LPCAT2*) and uridine monophosphate synthetase (*UMPS*) were identified to establish a prognosis signature. The risk score was determined as an independent prognostic indicator, and patients in the IRMPS-high group was strong linked with adverse prognosis for EC. Additionally, IRMPS was closely related with tumor immune infiltration. Notably, the IRMPS-low group had better immune checkpoint inhibitors (ICI) treatment response and more sensitive to chemotherapy drugs. **Conclusions**: In conclusion, IRMPS can serve as a precise prognostic tool to guide the personalized treatment of EC patients.

Keywords

Endometrial cancer; Immune; Metabolic; Immune infiltration; Immunotherapy; Prognostic signature

1. Introduction

Endometrial cancer (EC) is the sixth most frequent cancer among women worldwide, with an estimated over 410,000 new cases per year, even incidence and mortality are increasing [1]. Histopathological tumor grade categorization is vital for managing EC, allowing for prognostic segmentation into various risk groups, which guides surgical and adjuvant therapies. Specifically, the International Federation of Gynecology and Obstetrics defines grade 1 and 2 EECs as "low-grade" and grade 3 EECs as "high-grade" [2]. While a good five-year survival rate of approximately 90% is achieved by the majority of EC patients with early diagnosis [3, 4], some poorly-differentiated EC might return and have undesirable overcomes. Recent years, it is a great interest of the relationship among immune infiltration and metabolic reprogramming in malignancies. Therefore, comprehensively investigating the function of immune-related metabolic genes (IRMGs) implicated in EC progression is essential for prognostic prediction and treatment strategy.

Data-independent acquisition mass spectrometry (DIA-MS) based proteomics provides effective methods for assessing functional genes in cancer development. Several investigations confirmed the importance of the tumor microenvironment (TME) in cancer progression [5, 6]. Tumor cells undergo metabolic reprogramming to sustain continuous cell proliferation, a hallmark of cancer [7], which can be driven by matrix fibroblasts, immune cells and tumor cells

in the TME [8]. Additionally, metabolic remodeling can impact the phenotype and function of immune cells, and recent research has shown a strong link between phagocytosis performed tumor-associated macrophage (TAM) and oxidative phosphorylation (OXPHOS). Similar metabolic alterations were observed in tumor dendritic cells, leading to poor survival outcomes in lung cancer [9]. Previous reports have illustrated that cancer-associated fibroblasts (CAFs) may help with promoting tumor development and impacting on cancer metabolism in large part [10, 11]. Platten *et al.* [12] revealed that tryptophan metabolism was correlated with immunosuppression state in several cancers. Taken together, it is believed that tumor metabolic activity can influence the immune microenvironment and may serve a potential target for enhancing immunotherapy effectiveness.

At present, there are no reports on an immune-related metabolic prognosis signature (IRMPS) for EC patients, our main objective was to investigate the prognostic value of IRMPS for EC patients and to identify potential emerging therapeutic targets. We implemented a DIA-MS based proteomic approach using fresh frozen tumor samples from EC patients and identified 41 IRMGs. Then, using the TCGA-UCEC dataset, we developed a prediction model comprising 7 IRMGs: *NADUFA2*, *PRKAA2*, *STXBP1*, *NDUFB9*, *RPS27L*, *LPCAT2* and *UMPS*, based on which we observed that different risk groups exhibited distinct survival status, immune infiltration parameters and immunotherapy efficacy in EC patients. Overall, our proposed signature provides a foundation for enhancing the efficacy of treatment in EC.

2. Materials and methods

2.1 Patients and endometrium samples

We selected a total of 20 EC patients from the First Hospital of Lanzhou University involved 20 cancer tissues (CT, n = 20). Patients were classified as low-grade (grade 1–2, n = 10) or high-grade (grade 3, n = 10) based on the degree of tumor differentiation. The participants satisfied the following inclusion criteria: women $\geq$18 years with primary endometrial cancer. Excluded participants: (1) stage III–IV and non-endometrioid histological type; (2) absence of detailed clinical characteristics; (3) previous neoadjuvant chemotherapy, preoperative radiation or endocrine treatment; (4) history of malignancies or chronic diseases.

2.2 Sample preparation

We collected tissue within 30 min of removing the uterine appendages, immediately frozen it and stored it at −80 °C. Each sample of 20 μg tissues was directly dissolved in sodium dodecylsulfate (SDS) with dithiothreitol (DTT) (SDT buffer). Following centrifugation at 14,000g × 40 min, the protein concentrations were determined using BCA protein assay kit (PC0020, Solarbo, Beijing, China), then extracted and quantified peptides via filter-aided sample preparation (FASP).

2.3 Spectral library generation

A Q-Exactive orbitrap mass spectrometer equipped with an Easy nLC 1200 chromatography system (Q Exactive-HFX, Thermo Scientific, Waltham, MA, USA) was used to perform data-dependent acquisition (DDA). The peptide was first loaded onto a 75 μm I.D. ×2 cm trap column (C18, 3 μm, Thermo Scientific) with 95% of buffer A (0.1% formic acid in water), then separated on a 75 μm I.D. ×25 cm analytical column (C18, 2 μm, Thermo Scientific, Waltham, MA, USA) with a linear gradient of buffer B (84% acetonitrile and 0.1% formic acid). The peptide separation was carried out in 65 minutes at a flow rate of 300 nL/min using an LC procedure that started at 8% buffer B and progressed linearly up to 100% buffer B. Mass spectrometry (MS) spectra was collected in DDA mode using Q-Exactive HFX, which had the following parameters: a 300–1800 m/z scan range, a resolution of 60,000 at 200 m/z for mass spectrometry 1 (MS1), an automatic gain control (AGC) target of 3×10^6, a maximum injection time of 25 ms, and a dynamic exclusion of 30 s. After each MS1 scan, the top 20 precursor ions were selected for MS2. The maximum injection time was set to 25 ms, the AGC target value for the MS2 scan was 5×10^4, and the normalized collision energy was 30 eV.

2.4 DIA-MS/MS analysis

The DIA-MS/MS analysis was carried out in the same way as the DDA-MS/MS. The DIA was carried out using 30 isolation windows, covering a mass range of 350–1800 m/z at a resolution of 60,000, with an AGC target of 3×10^6 and a maximum injection duration of 50 ms. Spectronaut (SpectronautTM 14.4.200727, Biognosys, Switzerland) was used with default parameters to accomplish protein identification and quantification. All results were filtered based on a false discovery rate (FDR) of 1%.

2.5 DEGs identification and functional analysis

The criteria for identifying DEGs between high-grade cancer tissue (HG-CT) and low-grade cancer tissue (LG-CT) groups were "$p < 0.05$ and fold change (FC) >1.5 or <0.67". The volcano plot, principal component analysis (PCA), and heatmap with hierarchical clustering analysis were conducted using R package (R Version 3.4, R Foundation for Statistical Computing, Vienna, W, Austria) to get an overview of the DEGs characteristics. We conducted a gene enrichment analysis using Kyoto Encyclopedia of Genes and Genomes (KEGG), gene ontology (GO), and $p < 0.05$ was used as the limit for significantly enriched functional GO terms or KEGG pathways.

2.6 Screening of IRMGs

A total of 1793 genes associated to immunity and 1804 genes related to metabolism were obtained from the ImmPort database (https://www.immport.org/home) and previous report [13], respectively. Then, these genes were intersected with 285 differentially expressed genes (DEGs) which identified based on 20 fresh frozen cancer tissues to screen out 49 metabolic-DEGs and 20 immune-DEGs. To screen IRMGs,

the Spearman correlation was utilized ($p < 0.05$ and $|R| > 0.2$).

2.7 Development of immune-related metabolic prognosis signature (IRMPS)

Based on TCGA-UCEC dataset, we utilized the Lasso-cox regression analysis to establish a prognostic model, 7 IRMGs and their regression coefficients were obtained. The samples were split into high-risk and low-risk group based on the risk score median value. Subsequently, Kaplan-Meier (KM) survival curves and time-dependent receiver operational feature (ROC) curve analysis were performed to evaluate the predictive power of the signature. In order to identify prognosis-related genes, we subsequently employ univariate cox regression analysis. Multivariate cox regression analysis is then utilized to confirm the independence of the IRMPS model. The predictive value of the IRMPS and other clinical variables was also evaluated using the decision curve analysis (DCA) curve.

2.8 Construct of an IRMPS-based nomogram

According to the risk score and other clinical traits, such as age, stage, race and tumor grade, an IRMPS-based nomogram was created. Calibration plot was utilized to confirm the effectiveness of the nomogram.

2.9 Gene set enrichment analysis (GSEA)

We performed GSEA to investigate potential biological pathway and immunological activity related IRMPS. Normalized "$p < 0.05$" as meaningful enriched terms.

2.10 Immune-related analysis

We used the Tumor Immune Estimation Resource 2.0 (TIMER 2.0) (http://timer.cistrome.org/) to investigate the associations among IRMPS and six immune checkpoints in TCGA-UCEC. Immune Cell Abundance Identifier (ImmuCellAI) online tool (https://guolab.wchscu.cn/ImmuCellAI//#!/) was used to estimate the abundance of 24 immune cells in UCEC. The correlations between IRMPS model and 24 immune cells were evaluated by Spearman. Via ESTIMATE (https://bioinformatics.mdanderson.org/estimate/), we downloaded the ImmuneScore, StromalScore and ESTIMATEScore of TCGA-UCEC and calculated using "estimate" package.

2.11 Treatment response prediction

Using the tumor immune dysfunction and exclusion (TIDE) website (http://tide.dfci.harvard.edu/), we calculated TIDE scores, a novel approach for assessing immune checkpoint inhibitor (ICI) efficacy. Additionally, we investigated the relationship between immunophenoscore (IPS) and two risk groups in order to predict the value of this score in predicting the effectiveness of immunotherapy (program death protein 1 (PD-1)/program death ligand 1 (PD-L1) blockade and/or cytotoxic T-lymphocyte-associated antigen-4 (CTLA-4) blockade) on TCGA-UCEC patients by the Cancer Immunome Atlas (TCIA) (https://tcia.at/home).

To assess the sensibility of chemotherapy drugs, we utilized an open accessible database named Genomics of Drug Sensitivity in Cancer (GDSC) (https://www.cancerrxgene.org/), and estimate the half-maximal inhibitory concentration (IC50) for displaying the response to drugs.

2.12 Statistical analysis

Our data were tested for normality by using GraphPad Prism 9.0.0 software (GraphPad Software, San Diego, CA, USA). Comparisons between the two risk groups were assessed using Student's *t*-tests (passed normality test) or Wilcoxon rank sum tests (do not pass normality test). Statistically significant differences were defined as $*p < 0.05$, $**p < 0.01$ and $***p < 0.001$.

3. Results

3.1 Identification of DEGs in EC and biological function

We used DIA quantitative proteomics to analyze fresh frozen cancer tissues of 20 EC patients, comprised 10 high-grade and 10 low-grade. A total of 285 DEGs were collected ($p < 0.05$; fold change >1.5 or <0.67), including 148 up-regulated and 137 down-regulated (Fig. 1A and **Supplementary Table 1**). Fig. 1B showed an expression heatmap for 285 DEGs. The principal component analysis (PCA) was performed to compress the protein abundances in different samples into 20 two-dimensional data points, which were then displayed using a scatter plot (Fig. 1B). The figure revealed differences of protein abundance patterns between several sample groups, the PCA-derived distances can distinguish different tumor grades of EC (Fig. 1C). Further analyses of KEGG and GO enrichment demonstrated that the DEGs mainly involved in metabolic pathways, especially oxidative phosphorylation and formed electron transport chain (Fig. 2A–D).

3.2 Identification of IRMGs in EC

We collected 1804 metabolic genes and 1793 immune genes in order to identify the immune-related metabolic genes. Venn diagrams were performed to find 49 metabolic-DEGs and 20 immune-DEGs (Fig. 3A,B). Then, 41 IRMGs were screen by Spearman correlation analysis ($p < 0.05$, $|R| > 0.2$; Fig. 3C).

3.3 Development of an IRMPS with good performance in the TCGA dataset

Afterwards, we investigated whether the IRMGs could predict the survival of EC patients. A total of 41 IRMGs were selected to fit a LASSO regression model based on TCGA-UCEC (Fig. 4A). Then, we found the best lambda values ($\lambda = 0.0228$) via 10-fold cross-validation (Fig. 4B). Finally, 7 IRMGs were constructed be a prognosis signature and the risk scores were calculated as the following formula: risk score = $(-0.0264) \times NDUFA2 + (0.2147) \times PRKAA2 + (0.0146) \times STXBP1 + (0.0075) \times NDUFB9 + (-0.0401) \times RPS27L + (-0.2055) \times LPCAT2 + (0.049) \times UMPS$. In the TCGA-UCEC cohort, patients were divided into high-risk and low-risk categories. Fig. 4C showed the IRMPS can discriminate

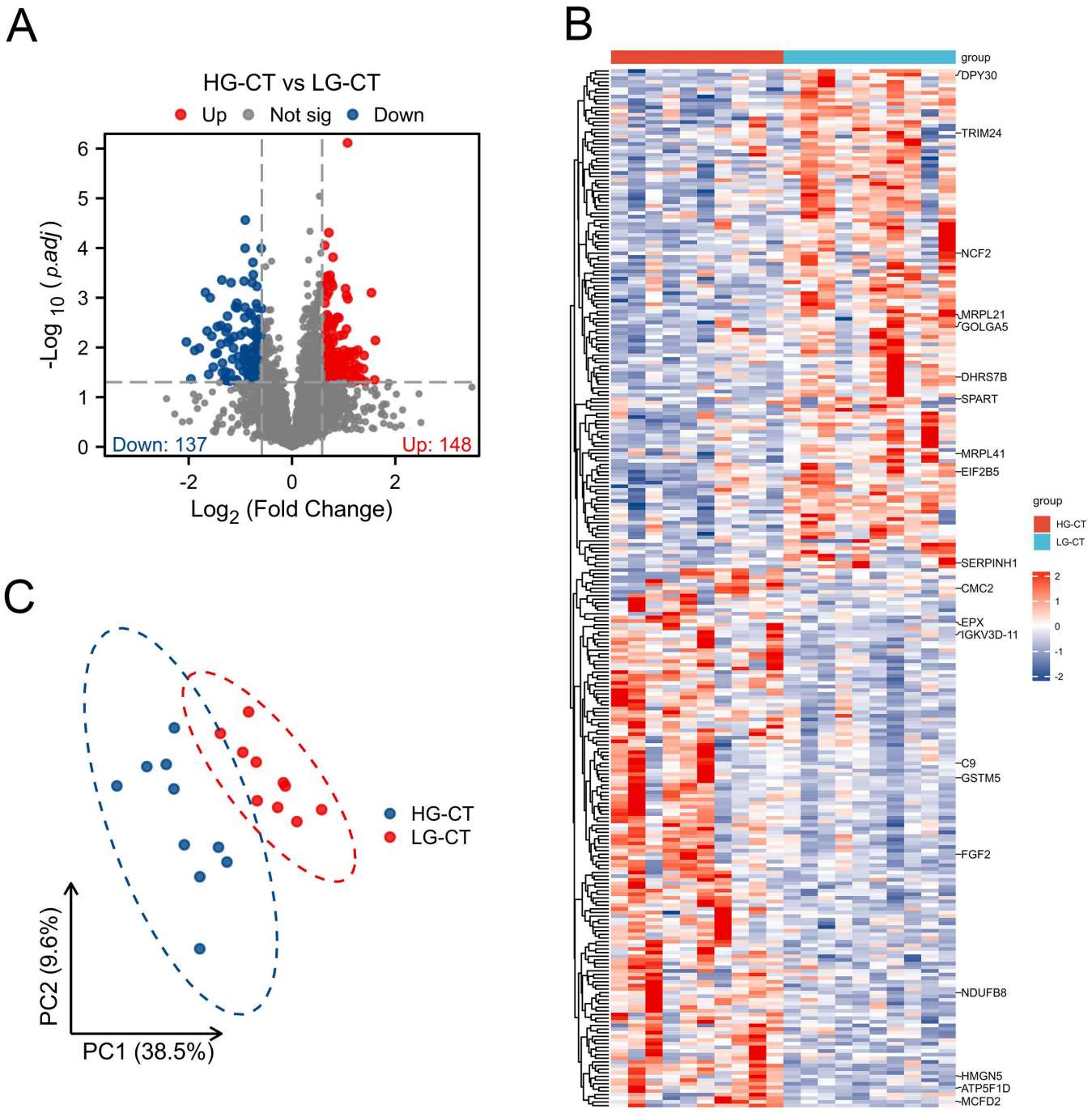

FIGURE 1. Proteomics analysis of differentially expressed genes (DEGs) in HG-CT groups compared to LG-CT groups of 20 EC patients. (A) Volcano plot of 285 DEGs, as follows: proteins presenting a fold change of more than 1.5 or less than 0.67 and $p < 0.05$. (B) Hierarchical clustering of 285 dysregulated proteins in tumors of different grades, and labeled the Top 10 up/down-regulated protein names. (C) PCA illustrating moderate clustering of tumor samples within each group. HG-CT: high-grade cancer tissue; LG-CT: low-grade cancer tissue; *DPY30*: Dpy-30 homolog; *TRIM24*: Tripartite motif containing 24; *NCF2*: Neutrophil cytosolic factor 2; *MRPL21*: Mitochondrial ribosomal protein L21; *GOLGA5*: Golgin A5; *DHRS7B*: Dehydrogenase/reductase (SDR family) member 7B; *SPART (SPG20)*: Spastic paraplegia 20; *MRPL41*: Mitochondrial ribosomal protein L41; *EIF2B5*: Eukaryotic translation initiation factor 2B, subunit 5; *SERPINH*: Serpin peptidase inhibitor, clade H (heat shock protein 47), member 1; *CMC2*: C-x(9)-C motif containing 2; *EPX*: Eosinophil peroxidase; *IGKV3D-11*: Immunoglobulin kappa variable 3D-11; *C9*: Complement component 9; *GSTM5*: Glutathione S-transferase mu 5; *FGF2*: Fibroblast growth factor 2; *NDUFB8*: NADH dehydrogenase (ubiquinone) 1 beta subcomplex, 8; *HMGN5*: High mobility group nucleosome binding domain 5; *ATP5F1D*: ATP synthase, H+ transporting, mitochondrial F1 complex; *MCFD2*: Multiple coagulation factor deficiency 2.

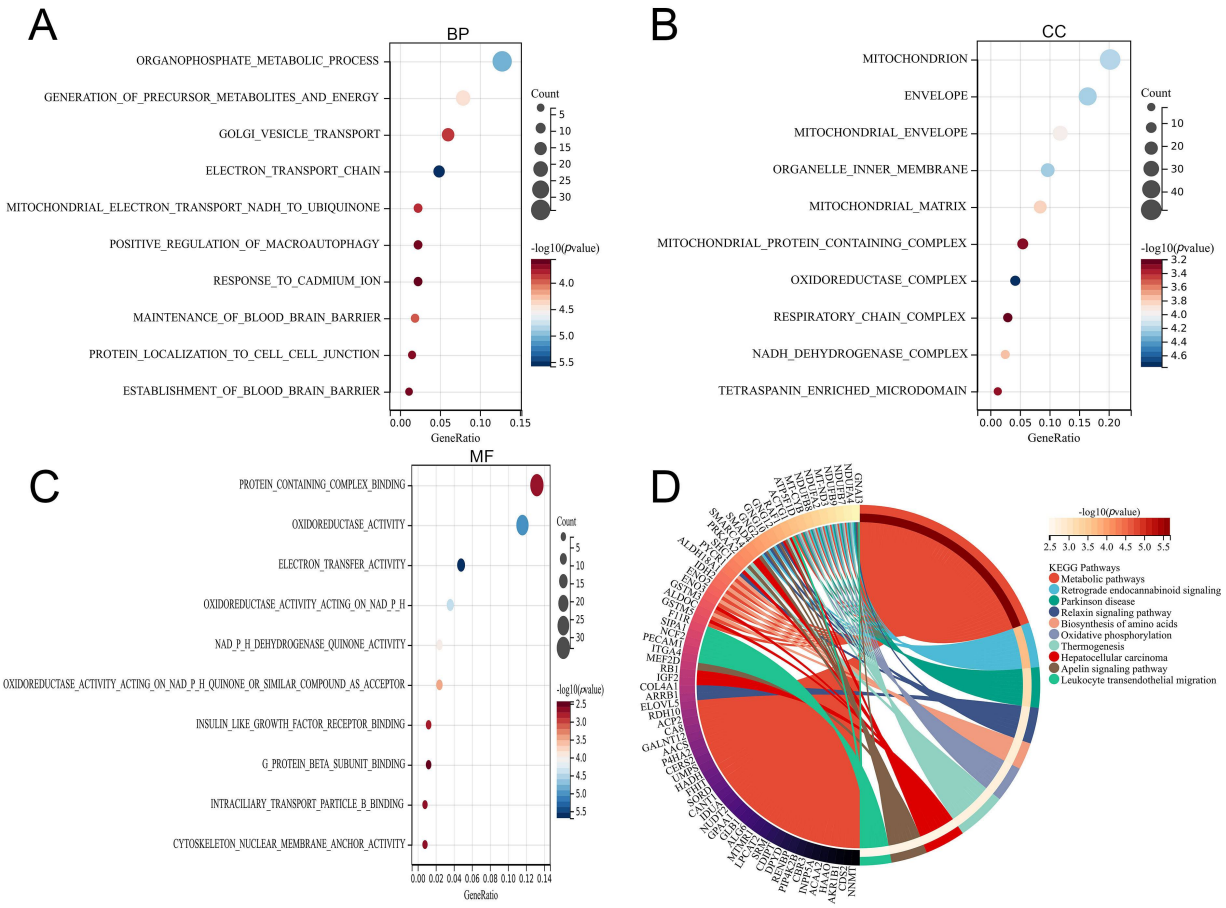

FIGURE 2. Function analysis of 285 DEGs. (A–C) Gene ontology (GO) functional annotation of 285 DEGs. (D) KEGG enrichment analysis of 285 DEGs. BP: biological process; CC: cellular component; MF: molecular function; *ITGA4*: Integrin alpha-4; *PECAM1*: Platelet endothelial cell adhesion molecule; *GNAI3*: Guanine nucleotide-binding protein G (I) subunit alpha-3; *SIPA1*: Signal-induced proliferation-associated protein 1; *F11R*: Junctional adhesion molecule A; *GNG2*: Guanine nucleotide-binding protein G (I); *PRKAA2*: 5′-AMP-activated protein kinase catalytic subunit alpha-2; *GNG10*: Guanine nucleotide-binding protein subunit gamma; *MEF2D*: MADS-box domain-containing protein; *GNG12*: Guanine nucleotide-binding protein subunit gamma; *SMAD4*: Mothers against decapentaplegic homolog 4; *RAF1*: RAF proto-oncogene serine; *ACTG1*: Actin, cytoplasmic 2; *IGF2*: Insulin-like growth factor II; *SHC1*: SHC-transforming protein 1; *GSTM3*: Glutathione S-transferase Mu 3; *RB1*: Retinoblastoma-associated protein; *SMARCA4*: SWI/SNF related, matrix associated, actin dependent regulator of chromatin, subfamily a, member 4; *NDUFA2*: NADH dehydrogenase (ubiquinone) 1 alpha subcomplex subunit 2; *MT-CYB*: Mitochondrially encoded cytochrome b; *MT-ND3*: NADH-ubiquinone oxidoreductase chain 3; *NDUFB9*: NADH dehydrogenase (ubiquinone) 1 beta subcomplex subunit 9; *NDUFB7*: NADH dehydrogenase (ubiquinone) 1 beta subcomplex subunit 7; *NDUFA4*: NADH dehydrogenase (ubiquinone) 1 alpha subcomplex subunit 4; *ALDOC*: Fructose-bisphosphate aldolase C; *ENO3*: Enolase 3 (beta, muscle); *ENO2*: Enolase 2 (gamma, neuronal); *IDH2*: Isocitrate dehydrogenase 2 (NADP+), mitochondrial; *ALDH18A1*: Delta-1-pyrroline-5-carboxylate synthase; *PYCR1*: Pyrroline-5-carboxylate reductase; *ARRB1*: Arrestin, beta 1; *COL4A1*: Collagen alpha-1 (IV) chain; *NNMT*: Nicotinamide N-methyltransferase; *CDS2*: CDP-diacylglycerol synthase (phosphatidate cytidylyltransferase) 2; *AKR1B1*: Aldo-keto reductase family 1 member B1; *HAAO*: 3-hydroxyanthranilate 3,4-dioxygenase; *ACAA2*: Acetyl-CoA acyltransferase 2; *INPP5A*: Inositol-polyphosphate 5-phosphatase; *CBR3*: Carbonyl reductase (NADPH); *PIP4K2B*: Phosphatidylinositol 5-phosphate 4-kinase type-2 beta; *RENBP*: GlcNAc 2-epimerase; *DPYD*: Dihydropyrimidine dehydrogenase; *CDIPT*: CDP-diacylglycerol-inositol 3-phosphatidyltransferase; *SRM*: Spermidine synthase; *LPCAT2*: Lysophosphatidylcholine acyltransferase 2; *MTMR1*: Myotubularin-related protein 1; *ALG6*: Dolichyl pyrophosphate Man9GlcNAc2 alpha-1,3-glucosyltransferase; *GLB1*: Nitrogen regulatory protein P-II homolog; *GPAA1*: Glycosylphosphatidylinositol anchor attachment 1 protein; *NUDT2*: Nudix (nucleoside diphosphate linked moiety X)-type motif 2; *IDUA*: Alpha-L-iduronidase; *CANT1*: Calcium activated nucleotidase 1; *SORD*: Sorbitol dehydrogenase; *FHIT*: Fragile histidine triad; *HADH*: Hydroxyacyl-CoA dehydrogenase; *UMPS*: Uridine monophosphate synthetase; *CERS2*: Ceramide synthase 2; *P4HA2*: Procollagen-proline 4-dioxygenase; *AACS*: Acetoacetyl-CoA synthetase; *GALNT12*: Polypeptide N-acetylgalactosaminyltransferase 12; *CA8*: Carbonic anhydrase VIII; *ACP2*: Acid phosphatase 2, lysosomal; *RDH10*: Retinol dehydrogenase 10; *ELOVL5*: Elongation of very long chain fatty acids protein 5.

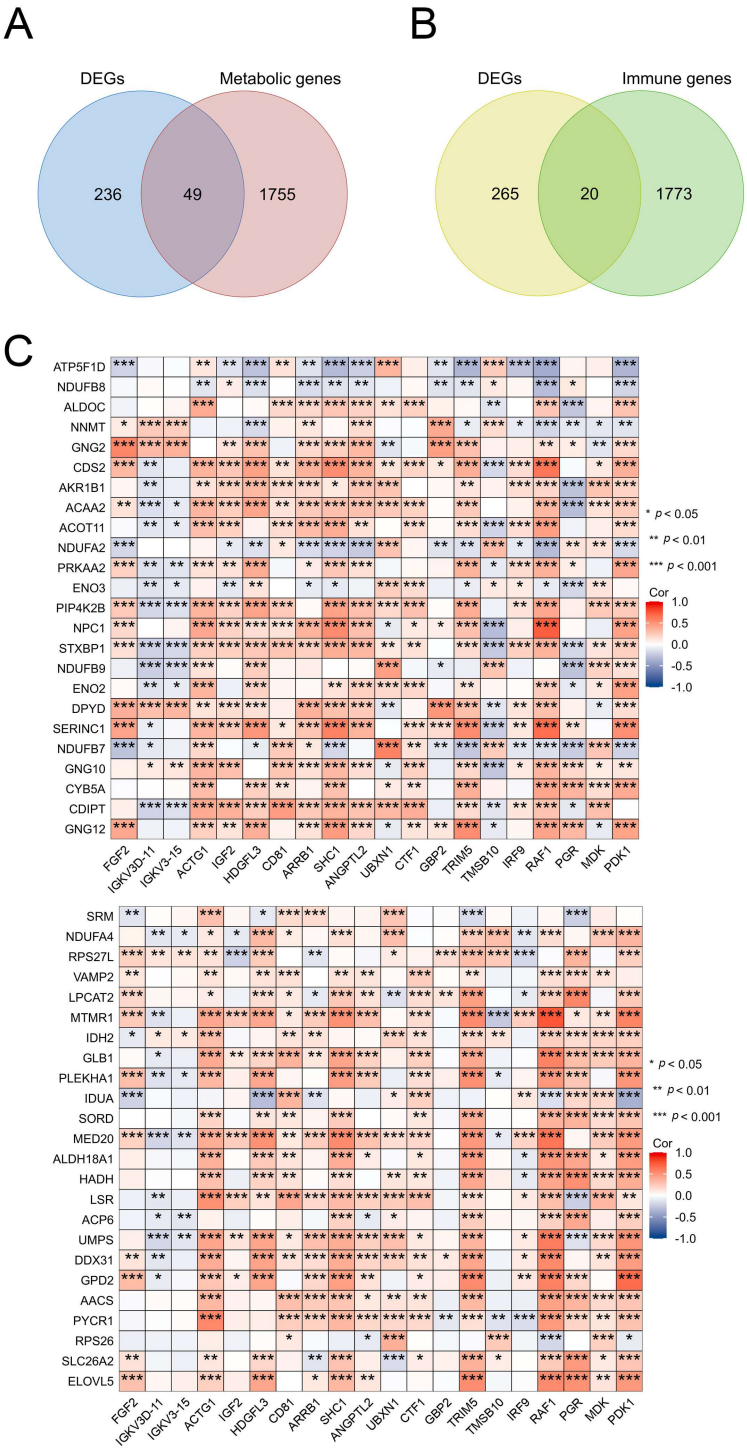

FIGURE 3. Screening immune-related metabolic genes (IRMGs). (A) Venn diagram of 49 metabolic-DEGs obtained based on the intersection between metabolic genes and DEGs. (B) Venn diagram of 20 immune-DEGs obtained based on the intersection between immune genes and DEGs. (C) The correlation between 49 metabolic-DEGs and 20 immune-DEGs in EC patients. *$p < 0.05$, **$p < 0.01$, ***$p < 0.001$. Cor: correlation; *ACOT11*: Acyl-coenzyme A thioesterase 11; *NPC1*: NPC intracellular cholesterol transporter 1; *STXBP1*: Syntaxin-binding protein 1; *SERINC1*: Serine incorporator 1; *CYB5A*: Cytochrome b5 heme-binding domain-containing protein; *RPS27L*: Ribosomal protein S27-like; *VAMP2*: Synaptobrevin-2; *PLEKHA1*: Pleckstrin homology domain-containing family A member 1; *MED20*: Mediator of RNA polymerase II transcription subunit 20; *LSR*: Lipolysis-stimulated lipoprotein receptor; *ACP6*: Lysophosphatidic acid phosphatase type 6; *DDX31*: DEAD (Asp-Glu-Ala-Asp) box polypeptide 31; *GPD2*: Glycerol-3-phosphate dehydrogenase, mitochondrial; *RPS26*: Ribosomal protein S26-like; *SLC26A2*: Sulfate transporter; *PDK1*: Protein-serine; *IGKV3-15*: Immunoglobulin kappa variable 3-15; *HDGFL3*: PWWP domain-containing protein; *CD81*: Tetraspanin; *ANGPTL2*: Angiopoietin-related protein 2; *UBXN1*: UBX domain-containing protein 1; *CTF1*: Cardiotrophin-1; *GBP2*: Guanylate-binding protein 2; *TRIM5*: Tripartite motif-containing protein 5; *TMSB10*: Thymosin beta-10; *IRF9*: Interferon regulatory factor 9; *PGR*: Progesterone receptor; *MDK*: Midkine.

risk scores, survival status and expression of 7 hub genes. According to the results of the Kaplan-Meier survival analysis, the risk-high group had a significantly lower overall survival (OS) rate versus the risk-low group ($p < 0.0001$; Fig. 4D), demonstrating the significance of the IRMPS in predicting the prognosis of EC patients. For one, three and five years of survival, the corresponding areas under the ROC curves (AUC) were 0.692, 0.717 and 0.731 (Fig. 4E), indicating satisfactory prediction model accuracy. Furthermore, a univariate cox regression model of the expression levels of the 7 prognostic genes (Fig. 5A) demonstrated that high expression of *PRKAA2* and *UMPS*, along with low expression of *NDUFA2*, *RPS27L* and *LPCAT2* were associated with poorer prognosis ($p < 0.05$; Fig. 5B). Collectively, these findings implied that the risk-scoring model may be used to predict the survival of EC patients.

3.4 The signature of seven immune-related metabolic genes might be an independent risk factor for EC

We used univariate and multivariate cox regression analysis to assess the independence of IRMPS for EC patients. The univariate cox analysis revealed that age, clinical stage, race, grade and risk score were important prognostic factors ($p < 0.001$; Fig. 6A). In addition, the risk score remained significant for prognosis in the multivariate cox analysis ($p = 0.001$; Fig. 6B), suggesting the IRMPS can be independent of other clinical features and should be incorporated into the establishment of prognostic models. A nomogram was created by merging other clinical parameters with the IRMPS model in order to further investigate the predictive capability of IRMPS (Fig. 6C). Afterward, the calibration curves showed powerful accuracy of the nomogram (Fig. 6D). DCA curve displayed that the prognostic value of IRMPS was superior than other clinical factors (Fig. 6E).

3.5 GSEA analysis and immune activity with different risk score

According to the GSEA analysis of IRMPS, several hallmarks were enriched, including kirsten rat sarcoma viral oncogene homolog (KRAS) signaling, xenobiotic metabolism, mitotic spindle and cell cycle checkpoints (G2/M) (Fig. 7A). Fig. 7B showed various of immunological pathways were related to the risk score, with substantial enrichment in the high-risk group.

Immune infiltration is a crucial factor related to tumor progression, and T cells are essential for the development, spread and treatment (especially immunotherapy) of cancer [14]. Through further comparison of the relationship between two risk groups and 24 tumor-infiltrating lymphocytes (TILs) abundances in EC via ImmuCellAI online tool, we observed that neutrophils, and Th2 cells were meaningfully positively associated with IRMPS ($p < 0.001$), while cytotoxic T cells (Tc), cluster of differentiation 8 (CD8)+ T cells, exhausted T cells (Tex), Th1 cells, T cell follicular helper (Tfh), natural killer (NK) cells and cluster of differentiation 4 (CD4)+ T cells were significantly negatively linked to IRMPS ($p < 0.001$; Fig. 8A). These findings proved that IRMPS is crucial for the immune infiltration of EC. Additionally, by comparing six immune checkpoint markers (PD1, CTLA4, PD-L1, PD-L2, lymphocyte activation gene-3 (LAG3) and hepatitis A virus-cellular receptor 2 (HAVCR2)) between the two risk groups, we discovered that IRMPS showed a remarkable negative correlation with CTLA4, PD-L1 and HAVCR2 ($p < 0.001$; Fig. 8B), indicating that an immune-suppressive microenvironment is more probable to form in low-risk groups.

3.6 Analysis of immunotherapy and chemotherapy response

Applying ESTIMATE methodology, we discovered that the IRMPS-high group had lower immune, stromal and ESTIMATE scores (Fig. 9A) while having higher tumor purity scores (Fig. 9B). The results implied that EC patients with high-risk IRMPS are associated with an environment that is more favorable for tumor growth. Through TCIA database, we found that the IRMPS-low group was significantly associated with higher IPS ($p < 0.05$) and IPS-CTLA4 ($p < 0.05$) scores (Fig. 9C). In the IRMPS model, we further generated the TIDE score to determine the effectiveness of immunotherapy. Lower TIDE scores suggest a lower likelihood of immune evasion, suggesting that patients may benefit from ICI therapy. In our analysis, low TIDE prediction scores were seen in the IRMPS-low group ($p < 0.01$; Fig. 9D), suggesting a better response to ICI therapy. However, the IRMPS-high group had higher exclusion ($p < 0.001$), myeloid-derived suppressor cell (MDSC) ($p < 0.001$), and tumor-associated macrophage (TAM) M2 ($p < 0.05$) scores, as well as a lower dysfunction score.

Chemotherapy is the most prevalent kind of treatment for EC patients. In our study, we forecasted the possibility that various chemotherapy medications would be effective via the GDSC database, then found that substantial variation in the IC50 between two risk groups among five chemotherapy medications. The IRMPS-low group were more sensitive to cisplatin, paclitaxel, vorinostat and vinorelbine, while the IRMPS-high group were more sensitive to bleomycin (Fig. 10).

3.7 Correlation analysis of four molecular subtypes and IRMPS model in EC

via TCGA-UCEC dataset, 545 EC patients were divided into four molecular subtypes, viz. polymerase-epsilon (POLE), microsatellite instability (MSI), copy number low and copy number high. After analyzing the correlation between four molecular subtypes and two risk groups, the prognosis signature was constituted of 7 immune-related metabolic genes, we found that the low-risk group had more MSI cases than IRMPS-high group (Fig. 11A). Fig. 11B displayed that EC patients with copy number high mainly manifested as high-grade histological type, and were distributed in IRMPS-high group more than IRMPS-low group. Then, we used TIMER database to investigate the infiltration level of 6 TILs in four molecular subtypes. The infiltration level of CD8+ T cells and dendritic cells were significantly highest in MSI, compared to other three molecular subtypes (Fig. 12A), indicating that MSI type endometrial cancer had more TILs abundance. We further explored the relationship among four molecular sub-

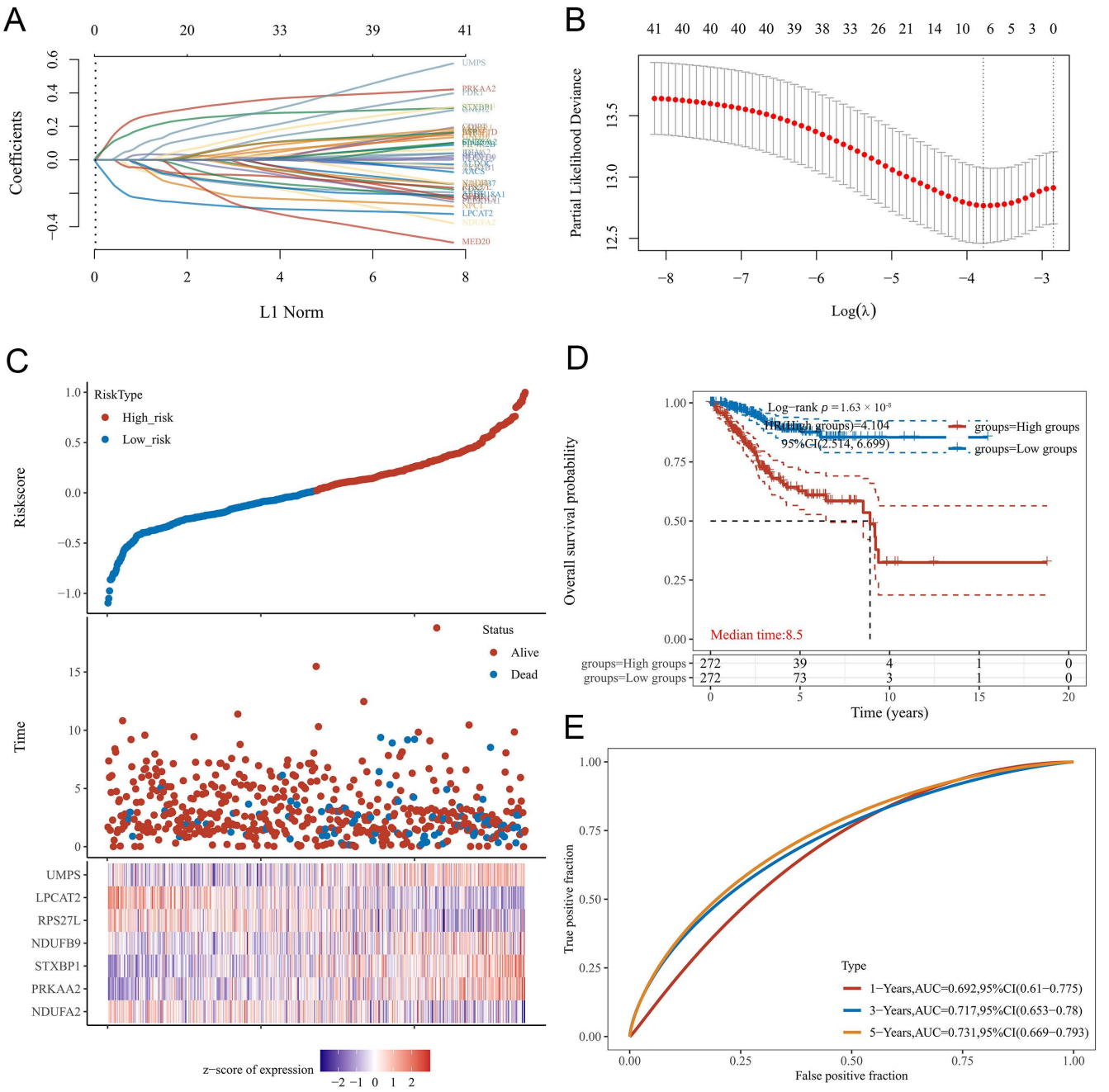

FIGURE 4. Construction of the immune-related metabolic gene prognostic model in TCGA-UCEC datasets. (A) prognostic IRMGs were evaluated using LASSO analysis and 10-fold cross validation. (B) Coefficient profile plots of 7 prognostic IRMGs. Vertical dashed lines are plotted at the best lambda. (C) Distribution of risk score, survival status and 7 hub gene expression. (D) Kaplan-Meier curves of overall survival between two risk groups in EC patients. (E) Time-dependent receiver operational feature (ROC) curves analysis of the prediction model. HR: Hazard Rate; AUC: Area Under the Curve; CI: Confidence Interval.

types with six immune checkpoint markers (PD-1, PD-L1, PD-L2, CTLA4, LAG3 and HAVCR2). The results demonstrated that the expression levels of PD-1, PD-L1, PD-L2, CTLA4 and LAG3 were meaningfully higher in MSI than other types (Fig. 12B), suggesting that immune checkpoint inhibitors may be effective against MSI type endometrial cancer. The four molecular subtypes did not significantly differ in their stromal, immune and ESTIMATE scores (Fig. 12C).

4. Discussion

As a result of early diagnosis techniques, the overall survival of EC patients has improved significantly, 20% of EC patients are still diagnosed with an advanced stage, which the survival probability declines to 10% [15, 16]. Hence, it is urgently needed for develop a prognostic model to improve the prognosis prediction of EC patients. In the current study, we concentrated on DIA-based proteomic characteristics combined

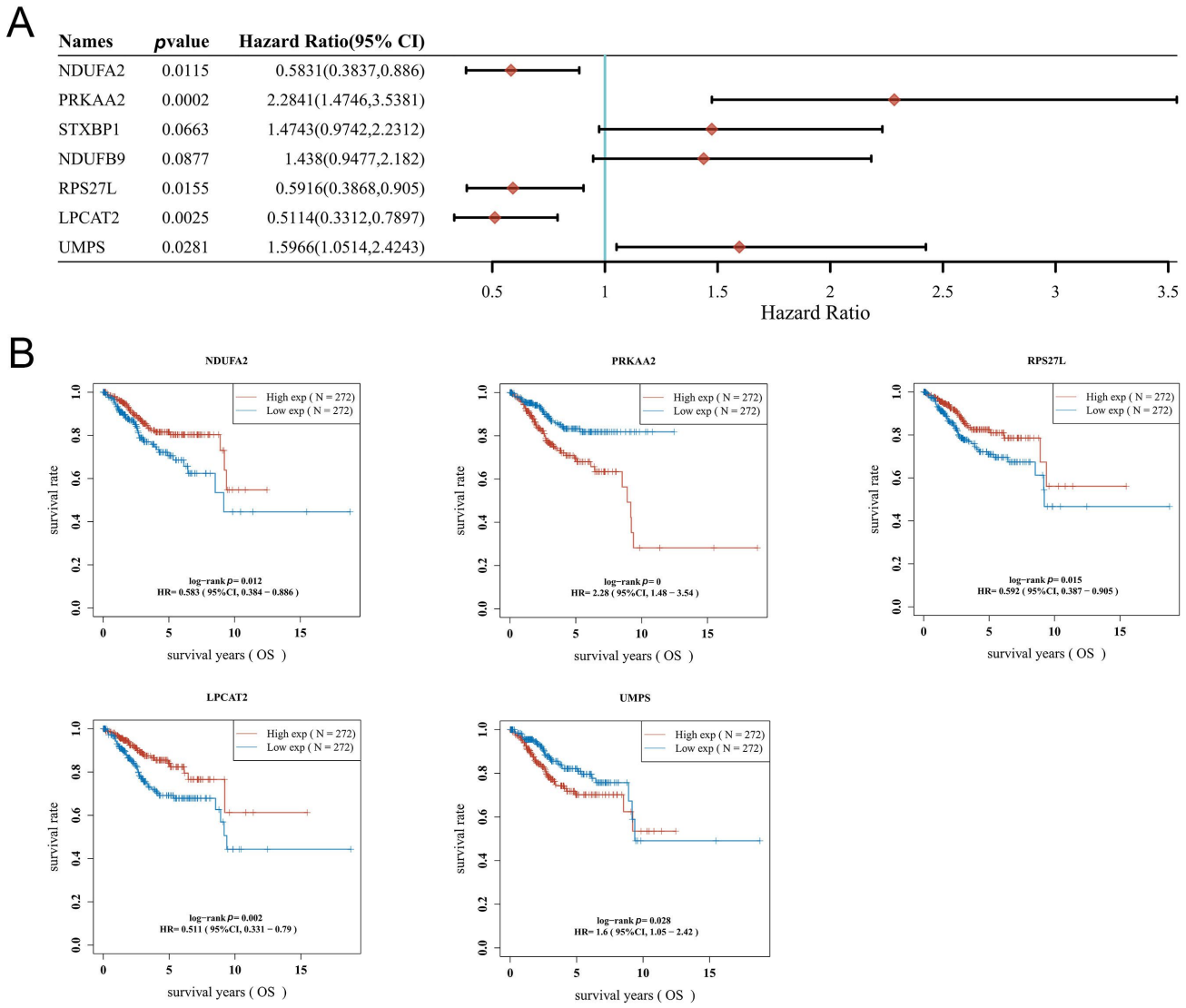

FIGURE 5. The hub genes of prognostic model. (A) The 7 hub genes screened out from LASSO in the TCGA-UCEC cohort were used to generate a forest plot of a univariate cox regression model. (B) Kaplan-Meier curves of *NDUFA2*, *PRKAA2*, *RPS27L*, *LPCAT2* and *UMPS*. High exp: High expression; Low exp: Low expression; *NDUFA2*: NADH dehydrogenase (ubiquinone) 1 alpha subcomplex subunit 2; *PRKAA2*: 5′-AMP-activated protein kinase catalytic subunit alpha-2; *STXBP1*: Syntaxin-binding protein 1; *NDUFB9*: NADH dehydrogenase (ubiquinone) 1 beta subcomplex subunit 9; *RPS27L*: Ribosomal protein S27-like; *LPCAT2*: Lysophosphatidylcholine acyltransferase 2; *UMPS*: Uridine monophosphate synthetase; OS: Overall Survival; CI: Confidence Interval; HR: Harzad Rate.

with TCGA-UCEC dataset, we screened out 285 DEGs, 41 IRMGs were determined, and created a prognostic signature comprising 7 hub genes for forecasting the survival and therapy response of EC patients, thereby providing valuable insights for personalized treatment strategies.

One of the current crucial aspects of cancer research and therapy is metabolic reprogramming, which supports a high proliferation rate and assure cell survival in the complex TME [17, 18]. However, immune cell could alter metabolic pathway and deeper impact on cellular phenotype and function [19]. Effective immune response depends on the proliferation, differentiation, and performance of immune cell effector activities, all of which involve metabolic reprogramming [8]. Based on the DIA-MS results, 285 DEGs were obtained, including 148 up-regulated and 137 down-regulated. We used DEGs intersected with immune-related and metabolic-related genes, respectively. Then, 41 IRM-DEGs were identified via the Spearman correlation analysis. According to the TCGA-UCEC project, we constructed a seven-gene prognostic signature, which could effectively predict survival outcomes, with the IRMPS-high group showing worse OS. The risk score was identified as an independent prognostic predictor of EC by univariate and multivariate cox regression analysis. To further explore the performance of IRMPS, we created an IRMPS-based nomogram incorporating age, clinic stage, race, tumor grade and risk score. The calibration curve displayed the nomogram was highly suitable for predicting prognosis. Also, DCA demonstrated that the prognostic capacity of IRMPS was more reliable than other clinical factors.

The IRMPS consisted of seven IRMGs, namely *NADUFA2*,

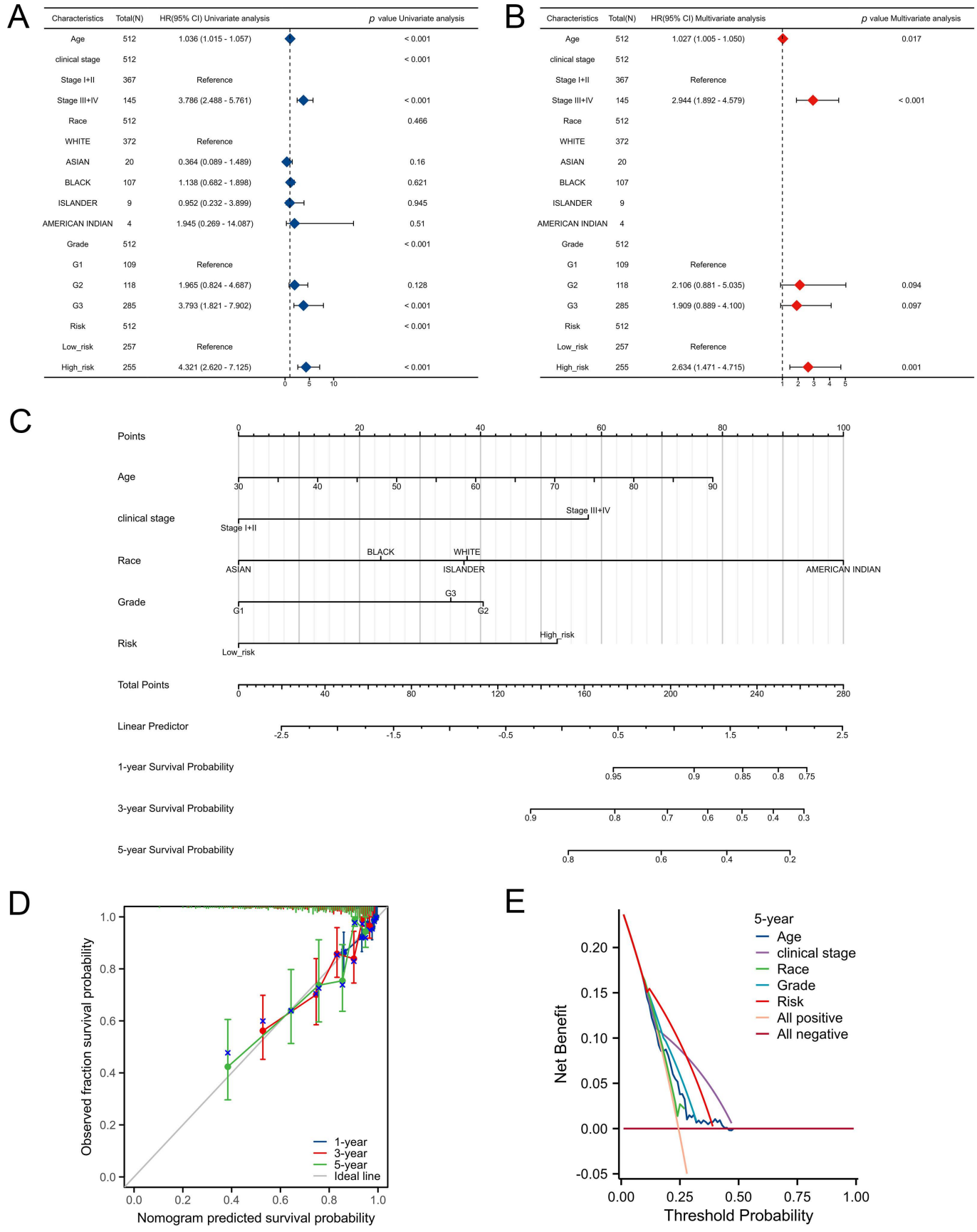

FIGURE 6. Construction and validation of a nomogram. Univariate (A) and multivariate cox regression (B) to assess the independence of the immune-related metabolic gene prognostic signature (IRMPS). (C) Nomogram for predicting the likelihood of 1-, 3- and 5-year OS of UCEC patients. (D) Nomogram calibration curves to forecast the likelihood of OS at 1-, 3- and 5-year. (E) The decision curve analysis (DCA) curves of IRMPS and other clinical characteristics for 5-year OS in UCEC patients. CI: Confidence Interval; HR: Harzad Rate.

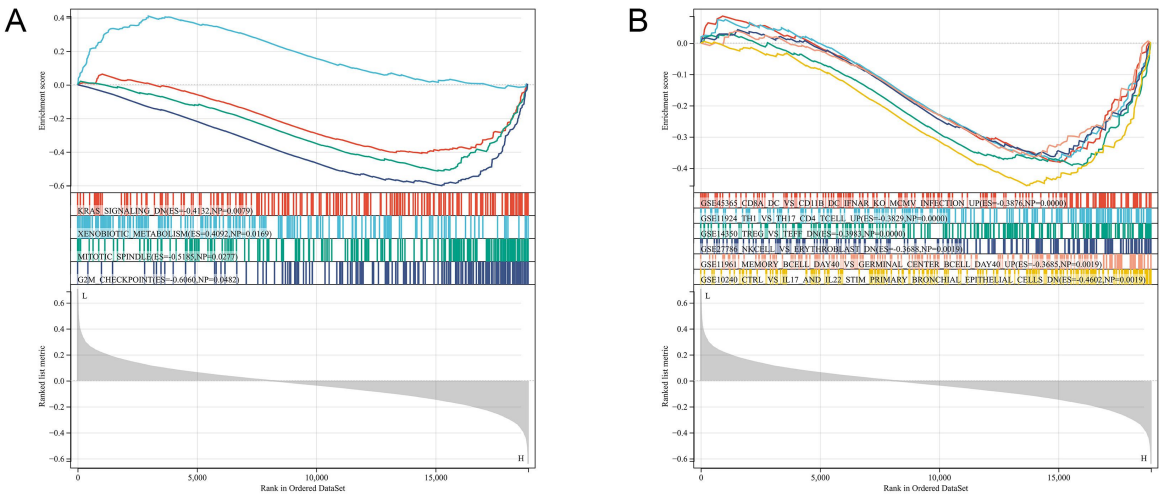

FIGURE 7. Gene set enrichment analysis. (A) Gene sets of hallmarks. (B) Gene sets of immune activity. L: low-risk group; H: high-risk group; ES: enrichment score; NP: nominal *p*-value.

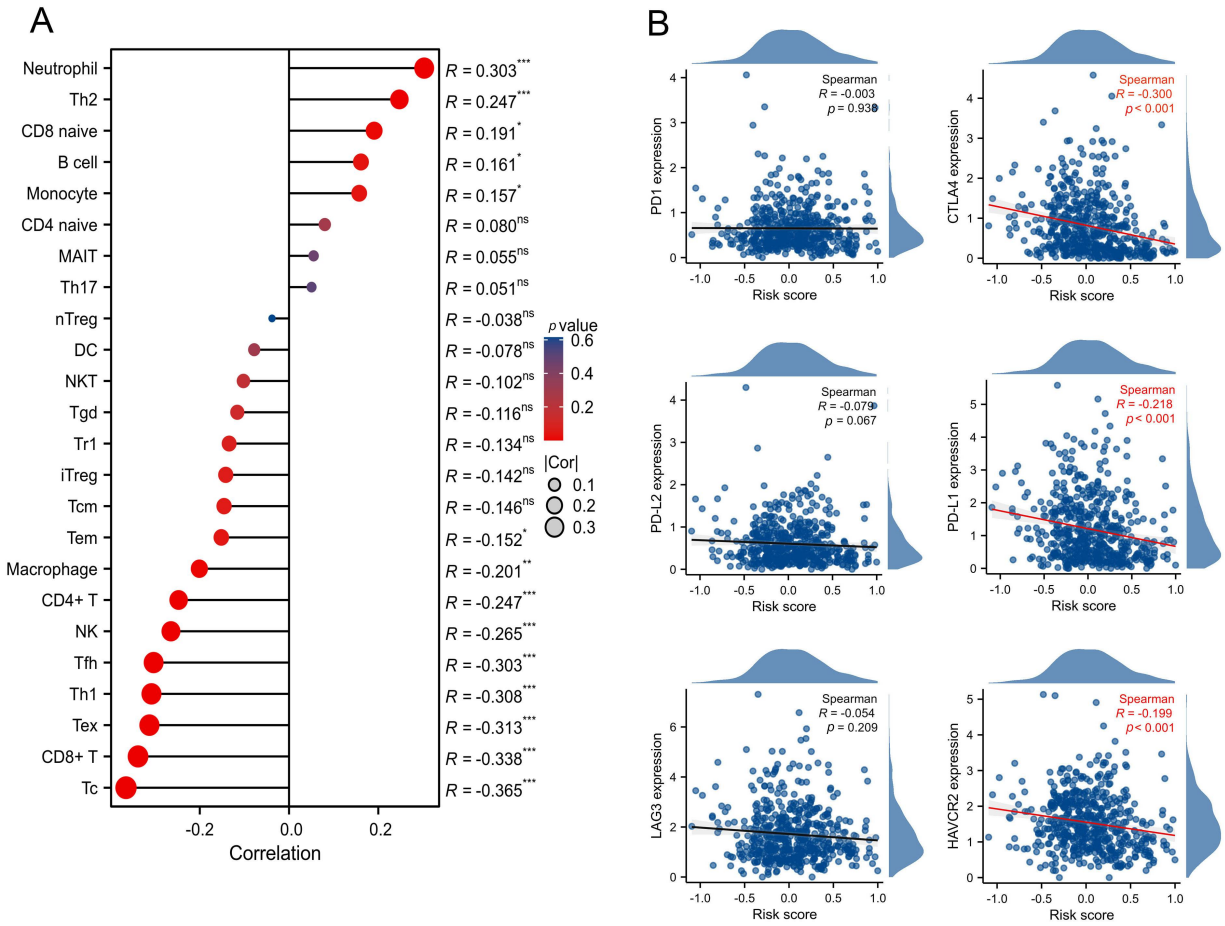

FIGURE 8. Immune activity analysis of the IRMPS model. (A) Correlation among the relative abundances of 24 tumor-infiltrating lymphocytes (TILs) and IRMPS model based on ImmuCellAI online tool. (B) Correlation between immune checkpoint and IRMPS model, including PD1, CTLA4, PD-L1, PD-L2, LAG3 and HAVCR2. *$p < 0.05$, **$p < 0.01$, ***$p < 0.001$. Th1: type I helper T cell; Th2: type II helper T cell; MAIT: mucosal-associated invariant T cell; NK: natural killer cell; NKT: natural killer T cell; DC: dendritic cells; Tgd: gamma delta T cell; Tcm: central memory T cell; Tem: effector memory T cell; Treg: regulatory T cell; Tr1: tregulatory1; Tc: cytotoxic T cell; CD8: cluster of differentiation 8; CD4: cluster of differentiation 4; Tex: exhausted T cell; Tfh: T cell follicular helper; PD-1: program death protein 1; PD-L1: program death ligand 1; PD-L2: program death ligand 2; CTLA-4: cytotoxic T-lymphocyte-associated antigen-4; LAG3: lymphocyte activation gene-3; HAVCR2: hepatitis A virus-cellular receptor 2; ^{ns}: non-significant.

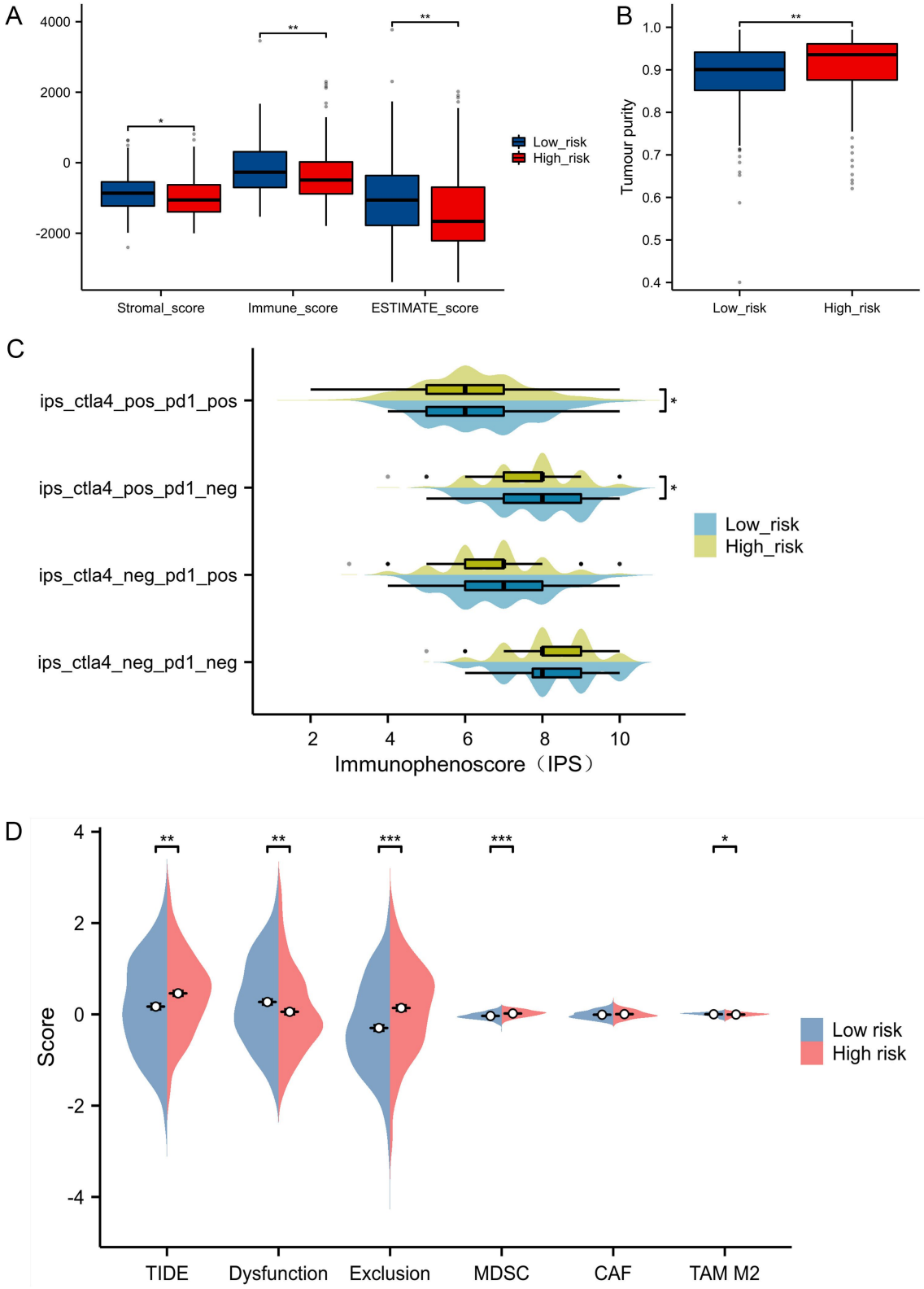

FIGURE 9. Analysis of immunotherapy response of EC patients. (A) The correlation between IRMPS model and Stromal Score, Immune Score and Estimate Score in TCGA-UCEC. (B) The correlation between IRMPS model and tumor purity. (C) The correlation between IRMPS model and IPS, IPS of PD-1/PD-L1 blocker, IPS of CTLA4 blocker, as well as IPS of CTLA4 and PD-1/PD-L1 blocker via TCIA website. (D) TIDE signatures predict checkpoint inhibitors (ICIs) immunotherapy response, along with dysfunction score, exclusion score, MDSC score, CAF score, TAM M2 score in two risk groups. *$p < 0.05$, **$p < 0.01$, ***$p < 0.001$. TIDE: tumor immune dysfunction and exclusion; MDSC: myeloid-derived suppressor cell; TAM MS: tumor-associated macrophage M2; CAF: cancer-associated fibroblasts; pos: positive; neg: negative.

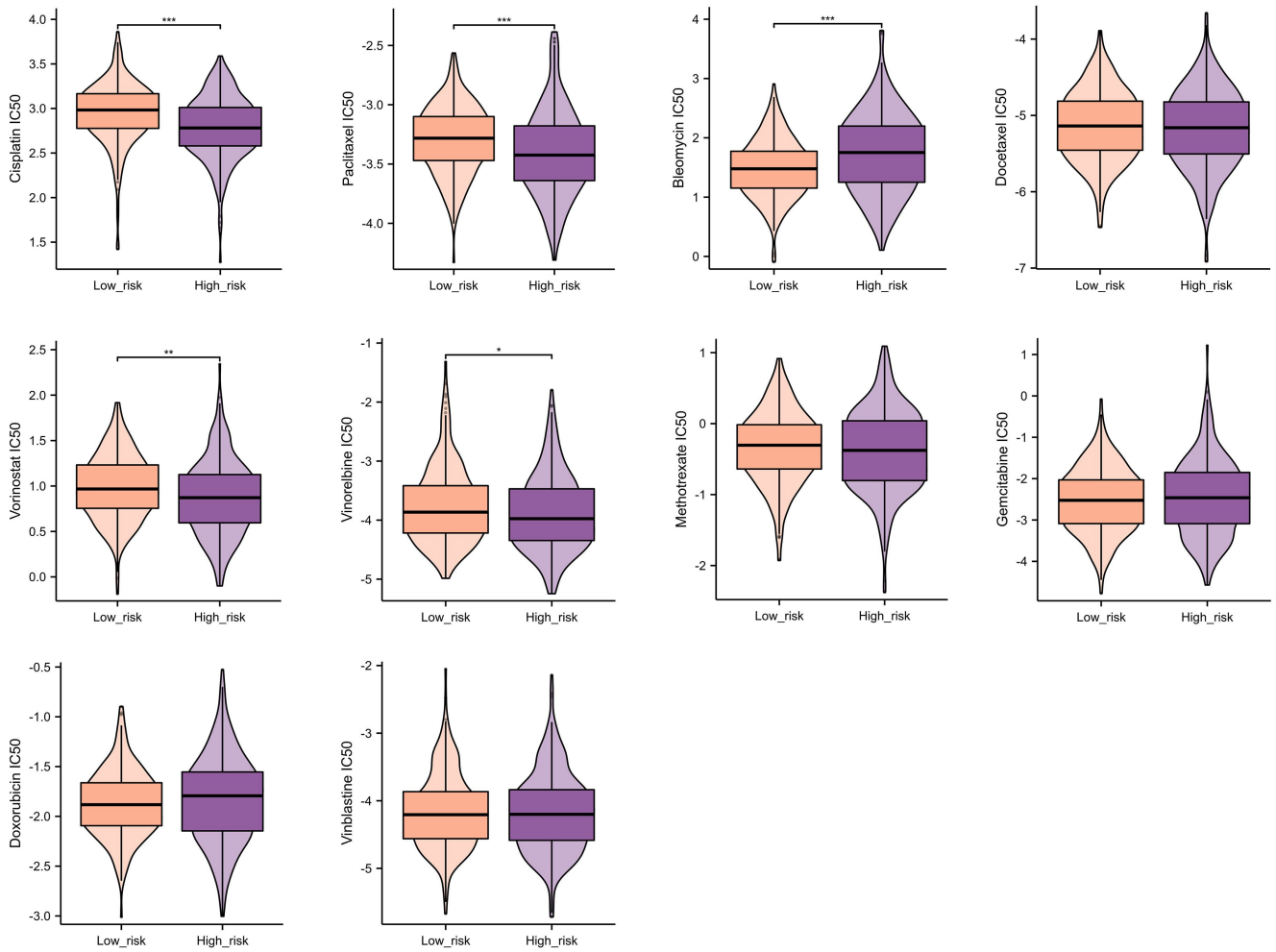

FIGURE 10. Analysis of chemotherapy response of EC patients. *$p < 0.05$, **$p < 0.01$, ***$p < 0.001$. IC50: half-maximal inhibitory concentration.

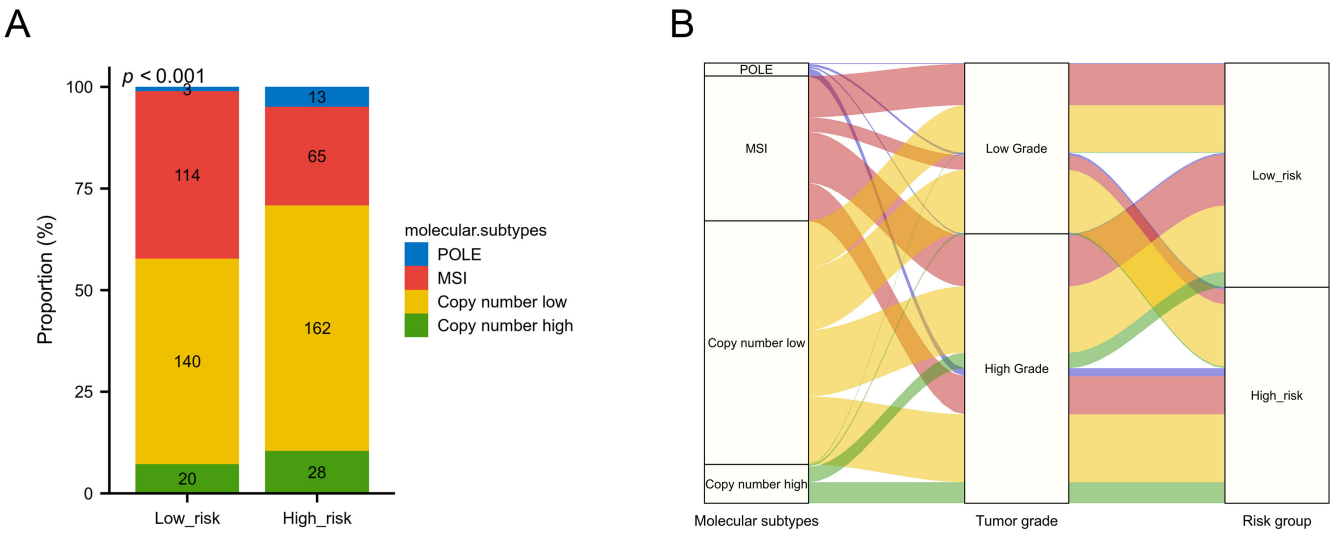

FIGURE 11. The correlation of four molecular subtypes, tumor grade and two risk groups in EC patients. (A) Distribution of four molecular subtypes in high and low risk groups. (B) The Sankey diagram of four molecular subtypes, tumor grade and two risk groups. POLE: polymerase-epsilon; MSI: microsatellite instability.

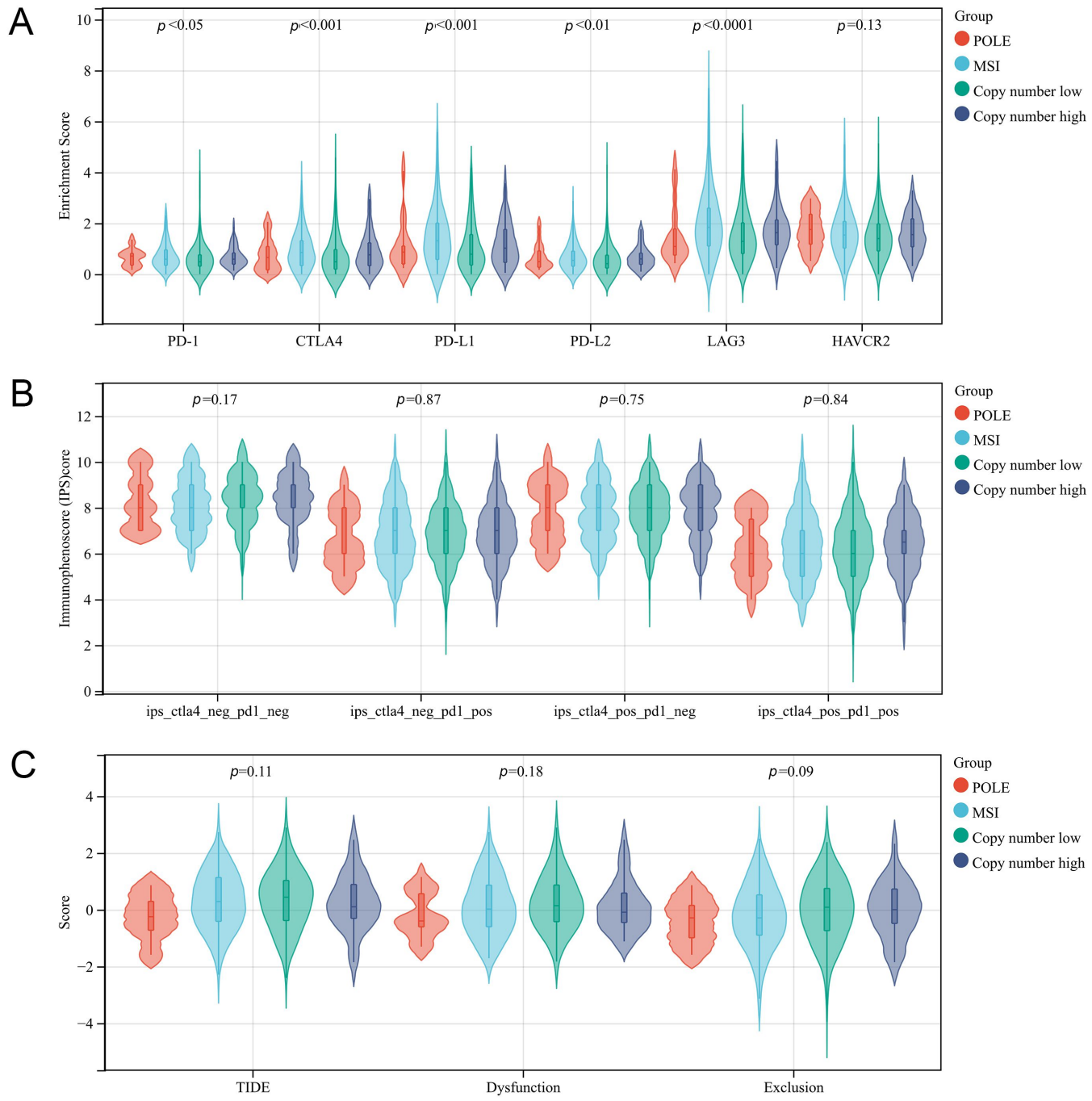

FIGURE 12. Immune activity analysis of the four molecular subtypes in EC. (A) The infiltration level of 6 TILs in four molecular subtypes based on TIMER database. (B) Correlation between immune checkpoint and four molecular subtypes, including PD-1, CTLA4, PD-L1, PD-L2, LAG3 and HAVCR2. (C) The correlation between four molecular subtypes and Stromal Score, Immune Score and Estimate Score in TCGA-UCEC. POLE: polymerase-epsilon; MSI: microsatellite instability; neg: negtive; pos: positive.

PRKAA2, *STXBP1*, *NDUFB9*, *RPS27*L, LPCAT2 and *UMPS*, all of which have been reported to have strong associations with tumors. In this study, we observed that the expression levels of these five signature genes within the IRMPS were significantly correlated with the survival outcomes of EC patients. Specifically, high expression of *PRKAA2* and *UMPS* was related to poor OS, while low expression of *NDUFA2*, *RPS27L* and *LPCAT2* was linked to favorable OS. *NDUFA2* and *NDUFB9* are auxiliary subunits of the mitochondrial membrane respiratory chain NADH dehydrogenase (complex I). Zhigang Wang *et al.* [20] demonstrated through mutational analysis of 14 patients that significant up-regulations of *NDUFA2*, *NDUFA10* and *NDUFA4* were involved in the development of head and neck paragangliomas (HNPGLs). *NDUFA2* has been found to be frequently targeted by tumorigenic microRNAs in colorectal cancer (CRC) [21]. *NDUFB9* has been reported to be down-regulated in highly metastatic breast cancer cells [22]. Furthermore, a bioinformatics anal-

ysis of uveal melanoma revealed that *NDUFB9*, acting as an oncogene-like gene, may be a prognostic factor in this type of cancer [23]. Similarly, *NDUFB9* was detected as an overexpressed gene that related to lymph node metastasis in esophageal squamous cell carcinoma (ESCC) [24]. It has been revealed that the AMP-activated protein kinase (AMPK) component *PRKAA2* is linked to adverse survival outcomes in both EC [25] and CRC [26]. *STXBP1* encodes a syntaxin-binding protein that modulates the release of neurotransmitters [27]. In lung cancer, *STXBP1* was found to be down-regulated but was identified as a prognosis-related gene in both lung squamous cell carcinoma (LUSC) and lung adenocarcinoma (LUAD) patients [28, 29]. *RPS27L* is a p53-repressible target [30]. In previous studies, it was reported to be downregulated in breast cancer [31] and CRC [32], which related with worse prognosis. Additionally, non-small cell lung cancer (NSCLC) showed decreased *RPS27L* expression and was associated with improved chemotherapy response [33]. *LPCAT2* was found to be overexpressed in cervical, breast, colon and esophageal cancers [34]. A study revealed that *LPCAT2* upregulation was related to adverse prognosis in cervical cancer patients [35]. *UMPS* has been reported to be closely linked to 5-FU-resistant in several kinds of tumors [36–38]. Furthermore, *UMPS* was found to be upregulated in hepatocellular carcinoma (HCC) and correlated with poor prognosis in affected patients [39].

To deeper explore the biological function of IRMPS, GSEA analysis was utilized, revealing activation of KRAS signaling, mitotic spindle and G2M checkpoint in the IRMPS-high group. Additionally, the high-risk group displayed a considerable enrichment of immune-related pathways. Zhang *et al.* [40] indicated that LINC01354 interacts with miR-216b to target KRAS, promoting EC progression. The mitotic spindle is believed to importantly act in tumor growth and development [41]. The G2M checkpoint facilitates DNA repair and can induce death in unrepaired cells [42].

We then detected the potential relationship between IRMPS and immunity, particularly regarding immune infiltration, immune checkpoint molecules and the TME. Numerous investigations have highlighted the importance of immune cells in growth and prognosis of tumors [43]. Here, our findings revealed a negative association between IRMPS and various T cell subtypes, such as Tc, CD8+ T cells, Tex, Th1 cells, Tfh and CD4+ T cells, indicating the strong immunoreactivity in the IRMPS-low group. T cells infiltration are essential for cancer occurrence, development and immunotherapy response [44]. CD8+ T cells and Tc play crucial roles as anti-tumor immune cells and have been shown to be involved in cell-killing mechanisms. As we known, CD4+ T cells and T helper cells (like Th1 and Tfh) can assist in immune effects. Increased infiltration of T helper cells has been shown to enhance the anti-tumor impactions of anti-CTLA-4 treatment against melanoma [45]. Vignali *et al.* [46] suggested that Tex exert the inhibitory function through CD39. The existing literature stated TME may encourage cancer development, spread and immunotherapy-resistant [47]. The IRMPS-low group, according to our findings, had higher stromal, immune and ESTIMATE scores, while IRMPS-high group had a higher tumor purity score. In addition, MDSC and TAM M2 as immunosuppressive cells, was found higher infiltration levels in the IRMPS-high group, making it a contributing factor to the worse OS observed in the IRMPS-high group compared to the IRMPS-low group. Collectively, our findings imply that IRMPS is essential for several TME components in EC patients.

Nowadays, immunotherapy has gained significant attention as a crucial treatment target for EC. Immune checkpoint markers are typical indicators assessing the therapeutic value of immunotherapy. Our co-expression analysis demonstrated that IRMPS was significantly negatively related to CTLA4, PD-L1 and HAVCR2. Moreover, IPS analysis indicated that the IRMPS-low group had a higher likelihood to benefit from CTLA-4 blockade, suggesting a favorable response to immunotherapy in this group. The IRMPS-low group also exhibited higher T cell infiltration, indicating a more immune-active or “hot” tumor environment, which may promote the efficacy of immunotherapy. Further analyses showed that the IRMPS-low group had higher T cell dysfunction score, while the IRMPS-high group had higher T cell exclusion score. These findings suggest that the two risk groups employ different immune evasion mechanisms, with the low-risk patients predominantly exhibiting T cell dysfunction while that of the high-risk patients operating mainly through T cell exclusion. Apart from immune checkpoint molecules and IPS, TIDE has emerged as a promising predictive method for ICI treatment response. In the current study, it is discovered that the IRMPS-low group had lower TIDE scores, indicating a higher likelihood of favorable responses to ICI treatment. Conversely, the high-risk group may enhance the risk of tumor immunity evasion and immunotherapy-resistant of EC patients.

Otherwise, chemotherapy was another common therapy option for EC. Based on the estimated IC50 results, EC patients in the low-risk group were more sensitive to four chemo drugs: cisplatin, paclitaxel, vorinostat and vinorelbine. In contrast, the high-risk group demonstrated resistance to these chemo drugs, which may account for their dismal prognosis.

After analyzing the correlation between four molecular subtypes and two risk groups, we discovered that the IRMPS-low group had a larger percentage of EC patients with the MSI subtype, while the IRMPS-high group had more copy number high EC subtype. As we known, copy number high EC patients with the worst prognosis [48]. Previous studies have indicated that MSI type was observed relatively high percentages of CD8+ T cells [49] and could benefit a lot from ICI [50, 51], which was consistent with the results we have found. These findings confirm once again that EC patients in the low-risk group could be the potential ICI treatment candidates. However, EC patients in the high-risk group with more copy number high cases had unfavorable prognosis.

Indeed, this study has limitations as well. To confirm our findings and the robustness of this immunometabolic prognostic model, numerous prospective clinical investigations are needed. To validate this approach, additional clinical trials would be more persuasive. To bolster our findings, more in-depth fundamental investigations (both *in vitro* and *in vivo*) should be planned.

5. Conclusions

In conclusion, our study established a novel immune-related metabolic signature in EC, which demonstrated excellent performance in prognostic prediction. Strikingly, EC patients in the IRMPS-low group exhibited higher levels of T cell infiltration and showed better responses to both immunotherapy and chemotherapy. The findings suggested that the IRMPS had the potential to predict prognosis in EC and also provides valuable insights into the immune microenvironment status, guiding future research in exploring therapeutic alternatives for EC patients.

AVAILABILITY OF DATA AND MATERIALS

The data that support the findings of this study are available from the corresponding author upon reasonable request.

AUTHOR CONTRIBUTIONS

YMC, PYY—conceptualization, investigation; YMC—methodology, software, validation, formal analysis, data curation, writing–original draft preparation, writing–review and editing, visualization, supervision; YXY, XLL—resources; YMC, XLL—project administration; YMC, YXY, XLL—funding acquisition. All authors have read and agreed to the published version of the manuscript.

ETHICS APPROVAL AND CONSENT TO PARTICIPATE

The study was conducted in accordance with the Declaration of Helsinki, and approved by the Ethics Committee of the First Hospital of Lanzhou University (ethical code: LDYYLL2021-310 and date of approval: 13 October 2021). Informed consent was obtained from all subjects involved in the study.

ACKNOWLEDGMENT

Not applicable.

FUNDING

This research was supported by the National Natural Science Foundation of China (No. 81960278), the Outstanding Youth Funds of Science and Technology Department of Gansu Province (No. 20JR5RA371), the Outstanding Youth Funds of Science and Technology Department of Gansu Province (No. 21JR7RA383), the Intra-Hospital Funds of the First Hospital of Lanzhou University (No. ldyyyn2021-2), the Medical Innovation and Development Project of Lanzhou University (lzuyxcx-2022-200), the Youth Science Fund of the First Hospital of Lanzhou University (No. ldyyyn2021-57).

CONFLICT OF INTEREST

The authors declare no conflict of interest.

SUPPLEMENTARY MATERIAL

Supplementary material associated with this article can be found, in the online version, at https://oss.ejgo.net/files/article/1702582291495043072/attachment/Supplementary%20material.xlsx.

REFERENCES

[1] Sung H, Ferlay J, Siegel RL, Laversanne M, Soerjomataram I, Jemal A, *et al*. Global cancer statistics 2020: GLOBOCAN estimates of incidence and mortality worldwide for 36 cancers in 185 countries. CA: A Cancer Journal for Clinicians. 2021; 71: 209–249.

[2] Oaknin A, Bosse TJ, Creutzberg CL, Giornelli G, Harter P, Joly F, *et al*. Endometrial cancer: ESMO clinical practice guideline for diagnosis, treatment and follow-up. Annals of Oncology. 2022; 33: 860–877.

[3] Shen Y, Yang W, Liu J, Zhang Y. Minimally invasive approaches for the early detection of endometrial cancer. Molecular Cancer. 2023; 22: 53.

[4] Safdar NS, Stasenko M, Selenica P, Martin AS, da Silva EM, Sebastiao APM, *et al*. Genomic determinants of early recurrences in low-stage, low-grade endometrioid endometrial carcinoma. Journal of the National Cancer Institute. 2022; 114: 1545–1548.

[5] Zou W, Green DR. Beggars banquet: metabolism in the tumor immune microenvironment and cancer therapy. Cell Metabolism. 2023; 35: 1101–1113.

[6] Bejarano L, Jordão MJC, Joyce JA. Therapeutic targeting of the tumor microenvironment. Cancer Discovery. 2021; 11: 933–959.

[7] Raggi C, Taddei ML, Rae C, Braconi C, Marra F. Metabolic reprogramming in cholangiocarcinoma. Journal of Hepatology. 2022; 77: 849–864.

[8] Zhao X, Li K, Chen M, Liu L. Metabolic codependencies in the tumor microenvironment and gastric cancer: difficulties and opportunities. Biomedicine & Pharmacotherapy. 2023; 162: 114601.

[9] Gonzalez MA, Lu DR, Yousefi M, Kroll A, Lo CH, Briseño CG, *et al.* Phagocytosis increases an oxidative metabolic and immune suppressive signature in tumor macrophages. Journal of Experimental Medicine. 2023; 220: e20221472.

[10] Zhou H, Zhang Y, Zhang R, Zhao M, Chen W, Liu Y, *et al.* A tumor-microenvironment-activatable molecular pro-theranostic agent for photodynamic and immunotherapy of cancer. Advanced Materials. 2023; 35: e2211485.

[11] Guo D, Ji X, Xie H, Ma J, Xu C, Zhou Y, *et al*. Targeted reprogramming of vitamin B_3 metabolism as a nanotherapeutic strategy towards chemoresistant cancers. Advanced Materials. 2023; 35: e2301257.

[12] Platten M, Nollen EAA, Röhrig UF, Fallarino F, Opitz CA. Tryptophan metabolism as a common therapeutic target in cancer, neurodegeneration and beyond. Nature Reviews Drug Discovery. 2019; 18: 379–401.

[13] Li F, Huang C, Qiu L, Li P, Shi J, Zhang G. Comprehensive analysis of immune-related metabolic genes in lung adenocarcinoma. Frontiers in Endocrinology. 2022; 13: 894754.

[14] Miao YR, Zhang Q, Lei Q, Luo M, Xie GY, Wang H, *et al*. ImmuCellAI: a unique method for comprehensive T-cell subsets abundance prediction and its application in cancer immunotherapy. Advanced Science. 2020; 7: 1902880.

[15] van Weelden WJ, Lalisang RI, Bulten J, Lindemann K, van Beekhuizen HJ, Trum H, *et al*. Impact of hormonal biomarkers on response to hormonal therapy in advanced and recurrent endometrial cancer. American Journal of Obstetrics and Gynecology. 2021; 225: 407.e1–407.e16.

[16] He Y, Shi Y, Yang Y, Huang H, Feng Y, Wang Y, *et al*. Chrysin induces autophagy through the inactivation of the ROS-mediated Akt/mTOR signaling pathway in endometrial cancer. International Journal of Molecular Medicine. 2021; 48: 172.

[17] Zheng P, Lin Z, Ding Y, Duan S. Targeting the dynamics of cancer metabolism in the era of precision oncology. Metabolism. 2023; 145: 155615.

[18] Tan YQ, Zhang X, Zhang S, Zhu T, Garg M, Lobie PE, *et al*. Mitochondria: the metabolic switch of cellular oncogenic transformation. Biochimica et Biophysica Acta—Reviews on Cancer. 2021; 1876:

188534.

[19] Hortová-Kohoutková M, Lázničková P, Frič J. How immune-cell fate and function are determined by metabolic pathway choice: the bioenergetics underlying the immune response. BioEssays. 2021; 43: e2000067.

[20] Wang Z, Chen H, Xue L, He W, Shu W, Wu H, *et al.* High throughput proteomic and metabolic profiling identified target correction of metabolic abnormalities as a novel therapeutic approach in head and neck paraganglioma. Translational Oncology. 2021; 14: 101146.

[21] Shi Y, Zhuang Y, Zhang J, Chen M, Wu S. Identification of tumorigenic and prognostic biomarkers in colorectal cancer based on microRNA expression profiles. BioMed Research International. 2020; 2020: 7136049.

[22] Li LD, Sun HF, Liu XX, Gao SP, Jiang HL, Hu X, *et al*. Down-regulation of NDUFB9 promotes breast cancer cell proliferation, metastasis by mediating mitochondrial metabolism. PLOS ONE. 2015; 10: e0144441.

[23] Choi S, Ha M, Lee JS, Heo HJ, Kim GH, Oh SO, *et al*. Novel prognostic factor for uveal melanoma: bioinformatics analysis of three independent cohorts. Anticancer Research. 2020; 40: 3839–3846.

[24] Uchikado Y, Inoue H, Haraguchi N, Mimori K, Natsugoe S, Okumura H, *et al*. Gene expression profiling of lymph node metastasis by oligomicroarray analysis using laser microdissection in esophageal squamous cell carcinoma. International Journal of Oncology. 2006; 29: 1337–1347.

[25] Weijiao Y, Fuchun L, Mengjie C, Xiaoqing Q, Hao L, Yuan L, *et al.* Immune infiltration and a ferroptosis-associated gene signature for predicting the prognosis of patients with endometrial cancer. Aging. 2021; 13: 16713–16732.

[26] Zhang Q, Hong Z, Zhu J, Zeng C, Tang Z, Wang W, *et al*. miR-4999-5p predicts colorectal cancer survival outcome and reprograms glucose metabolism by targeting PRKAA2. OncoTargets and Therapy. 2020; 13: 1199–1210.

[27] Lu Z, He S, Jiang J, Zhuang L, Wang Y, Yang G, *et al*. Base-edited cynomolgus monkeys mimic core symptoms of STXBP1 encephalopathy. Molecular Therapy. 2022; 30: 2163–2175.

[28] Wang X, Fu G, Wen J, Chen H, Zhang B, Zhu D. Membrane location of syntaxin-binding protein 1 is correlated with poor prognosis of lung adenocarcinoma. The Tohoku Journal of Experimental Medicine. 2020; 250: 263–270.

[29] Yu M, Tian Y, Wu M, Gao J, Wang Y, Liu F, *et al*. A comparison of mRNA and circRNA expression between squamous cell carcinoma and adenocarcinoma of the lungs. Genetics and Molecular Biology. 2020; 43: e20200054.

[30] Xu AF, Molinuevo R, Fazzari E, Tom H, Zhang Z, Menendez J, *et al*. Subfunctionalized expression drives evolutionary retention of ribosomal protein paralogs *Rps27* and *Rps27l* in vertebrates. eLife. 2023; 12: e78695.

[31] Xiong X, Liu X, Li H, He H, Sun Y, Zhao Y. Ribosomal protein S27-like regulates autophagy via the β-TrCP-DEPTOR-mTORC1 axis. Cell Death & Disease. 2018; 9: 1131.

[32] Huang CJ, Yang SH, Lee CL, Cheng YC, Tai SY, Chien CC. Ribosomal protein S27-like in colorectal cancer: a candidate for predicting prognoses. PLOS ONE. 2013; 8: e67043.

[33] Sun S, He H, Ma Y, Xu J, Chen G, Sun Y, *et al*. Inactivation of ribosomal protein S27-like impairs DNA interstrand cross-link repair by destabilization of FANCD2 and FANCI. Cell Death & Disease. 2020; 11: 852.

[34] Agarwal AK, Garg A. Enzymatic activity of the human 1-acylglycerol-3-phosphate-O-acyltransferase isoform 11: upregulated in breast and cervical cancers. Journal of Lipid Research. 2010; 51: 2143–2152.

[35] Souza JL, Martins-Cardoso K, Guimarães IS, de Melo AC, Lopes AH, Monteiro RQ, *et al*. Interplay between EGFR and the platelet-activating factor/PAF receptor signaling axis mediates aggressive behavior of cervical cancer. Frontiers in Oncology. 2020; 10: 557280.

[36] Yu S, Li Z, Tu L, Pu Y, Yan D, Wang X, *et al*. Uricase sensitizes hepatocellular carcinoma cells to 5-fluorouracil through uricase-uric acid-UMP synthase axis. Journal of Physiology and Biochemistry. 2022; 78: 679–687.

[37] Niu Y, Fan X, Wang Y, Lin J, Hua L, Li X, *et al.* Genome-wide CRISPR screening reveals pyrimidine metabolic reprogramming in 5-FU chronochemotherapy of colorectal cancer. Frontiers in Oncology. 2022; 12: 949715.

[38] Luo L, Zhang J, Tang H, Zhai D, Huang D, Ling L, *et al.* LncRNA SNORD3A specifically sensitizes breast cancer cells to 5-FU by sponging miR-185-5p to enhance UMPS expression. Cell Death & Disease. 2020; 11: 329.

[39] Yin L, He N, Chen C, Zhang N, Lin Y, Xia Q. Identification of novel blood-based HCC-specific diagnostic biomarkers for human hepatocellular carcinoma. Artificial Cells, Nanomedicine, and Biotechnology. 2019; 47: 1908–1916.

[40] Zhang Y, Zhao W, Na F, Li M, Tong S. LINC01354/microRNA-216b/KRAS axis promotes the occurrence and metastasis of endometrial cancer. Nanoscale Research Letters. 2022; 17: 21.

[41] Borys F, Tobiasz P, Poterała M, Fabczak H, Krawczyk H, Joachimiak E. Systematic studies on anti-cancer evaluation of stilbene and dibenzo[*b,f*]oxepine derivatives. Molecules. 2023; 28: 3558.

[42] Bucher N, Britten CD. G2 checkpoint abrogation and checkpoint kinase-1 targeting in the treatment of cancer. British Journal of Cancer. 2008; 98: 523–528.

[43] Yang Y, Lu T, Jia X, Gao Y. FSTL1 suppresses triple-negative breast cancer lung metastasis by inhibiting M2-like tumor-associated macrophage recruitment toward the lungs. Diagnostics. 2023; 13: 1724.

[44] Kochenderfer JN, Dudley ME, Kassim SH, Somerville RP, Carpenter RO, Stetler-Stevenson M, *et al*. Chemotherapy-refractory diffuse large B-cell lymphoma and indolent B-cell malignancies can be effectively treated with autologous T cells expressing an anti-CD19 chimeric antigen receptor. Journal of Clinical Oncology. 2015; 33: 540–549.

[45] Simpson TR, Li F, Montalvo-Ortiz W, Sepulveda MA, Bergerhoff K, Arce F, *et al*. Fc-dependent depletion of tumor-infiltrating regulatory T cells co-defines the efficacy of anti-CTLA-4 therapy against melanoma. Journal of Experimental Medicine. 2013; 210: 1695–1710.

[46] Vignali PDA, DePeaux K, Watson MJ, Ye C, Ford BR, Lontos K, *et al*. Hypoxia drives CD39-dependent suppressor function in exhausted T cells to limit antitumor immunity. Nature Immunology. 2023; 24: 267–279.

[47] Mathew AA, Zakkariya ZT, Ashokan A, Manohar M, Keechilat P, Nair SV, *et al*. 5-FU mediated depletion of myeloid suppressor cells enhances T-cell infiltration and anti-tumor response in immunotherapy-resistant lung tumor. International Immunopharmacology. 2023; 120: 110129.

[48] Bonazzi VF, Kondrashova O, Smith D, Nones K, Sengal AT, Ju R, *et al.* Patient-derived xenograft models capture genomic heterogeneity in endometrial cancer. Genome Medicine. 2022; 14: 3.

[49] Dai Y, Zhao L, Hua D, Cui L, Zhang X, Kang N, *et al*. Tumor immune microenvironment in endometrial cancer of different molecular subtypes: evidence from a retrospective observational study. Frontiers in Immunology. 2022; 13: 1035616.

[50] Oaknin A, Gilbert L, Tinker AV, Brown J, Mathews C, Press J, *et al*. Safety and antitumor activity of dostarlimab in patients with advanced or recurrent DNA mismatch repair deficient/microsatellite instability-high (dMMR/MSI-H) or proficient/stable (MMRp/MSS) endometrial cancer: interim results from GARNET—a phase I, single-arm study. Journal for ImmunoTherapy of Cancer. 2022; 10: e003777.

[51] Marabelle A, Le DT, Ascierto PA, Di Giacomo AM, De Jesus-Acosta A, Delord JP, *et al*. Efficacy of pembrolizumab in patients with noncolorectal high microsatellite instability/mismatch repair-deficient cancer: results from the phase II KEYNOTE-158 study. Journal of Clinical Oncology. 2020; 38: 1–10.

How to cite this article: Yuemei Cheng, Pingyuan Yu, Xiaolei Liang, Yongxiu Yang. Identification of an immune-related metabolic gene signature to predict possible prognosis in endometrial cancer and reveals immune landscape feature. European Journal of Gynaecological Oncology. 2025; 46(2): 47-63. doi: 10.22514/ejgo.2023.072.